ACS APPLIED MATERIALS & INTERFACES

www.acsami.org

Research Article

Annealing $Ti_3C_2T_z$ MXenes to Control Surface Chemistry and Friction

Kailash Arole, Stefano A. Micci-Barreca, Swarnima Athavale, Mohsen Tajedini, Greeshma Raghuvaran, Jodie L. Lutkenhaus, Miladin Radovic, Hong Liang, and Micah J. Green*

Cite This: *ACS Appl. Mater. Interfaces* 2024, 16, 6290−6300

Read Online

ACCESS | Metrics & More | Article Recommendations | Supporting Information

ABSTRACT: Although surface terminations (such as =O, −Cl, −F, and −OH) on MXene nanosheets strongly influence their functional properties, synthesis of MXenes with desired types and distribution of those terminations is still challenging. Here, it is demonstrated that thermal annealing helps in removing much of the terminal groups of molten salt-etched multilayered (ML) $Ti_3C_2T_z$. In this study, the chloride terminations of molten salt-etched ML-$Ti_3C_2T_z$ were removed via thermal annealing at increased temperatures under an inert (argon) atmosphere. This thermal annealing created some bare sites available for further functionalization of $Ti_3C_2T_z$. XRD, EDS, and XPS measurements confirm the removal of much of the terminal groups of ML-$Ti_3C_2T_z$. Here, the annealed ML-$Ti_3C_2T_z$ was refunctionalized by −OH groups and 3-aminopropyl triethoxysilane (APTES), which was confirmed by FTIR. The −OH and APTES surface-modified ML-$Ti_3C_2T_z$ are evaluated as a solid lubricant, exhibiting ∼70.1 and 66.7% reduction in friction compared to a steel substrate, respectively. This enhanced performance is attributed to the improved interaction or adhesion of functionalized ML-$Ti_3C_2T_z$ with the substrate material. This approach allows for the effective surface modification of MXenes and control of their functional properties.

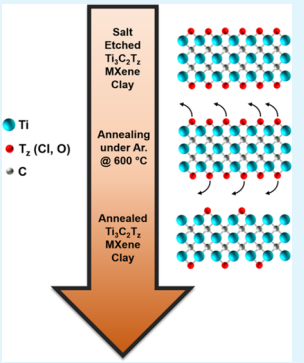

KEYWORDS: *2D nanomaterials, MXenes, annealing, surface modification, tribology, lubricant*

INTRODUCTION

Since their discovery by Naguib et al., MXenes have received considerable attention due to their exceptional properties, such as high thermal and electrical conductivity, and mechanical strength.[1−5] These outstanding properties are reported to be useful for many applications, including as energy storage, membranes, inks, and electromagnetic shielding.[6−17] MXenes have a general formula $M_{n+1}X_nT_z$ (n = 1−4), where M is an early transition metal (*e.g.*, Ti, V, Nb, Mo), X can be carbon or/and nitrogen, and T_z represents terminal groups such as −OH, =O, −F, −Cl, −Br, −I, and −S.[2,18,19] MXenes are obtained by the selective etching of the "A" (group 13−16 elements such as Al, Ga, Si) layer from the MAX phase precursor ($M_{n+1}AX_n$ where n = 1−4).[20−22] Around 50 types of MXenes have been reported, and more have been computed or synthesized, considering the possible compositions and solid solutions.[4,13,23]

MXene synthesis is usually carried out by utilizing various methods of wet enchanting parent MAX phases, most commonly using hydrofluoric acid (HF) as an etchant.[2,13,24] To minimize the dangers associated with HF, researchers have opted for safer approaches that use a mixture of HCl and various inorganic and organic salts such as lithium fluoride (LiF), ammonium bifluoride (NH_4HF_2), and tetramethylammonium-fluoride (TMAF).[25−27] Although the acid etching (HF) method is more commonly used to etch MXenes, the hazards associated with handling concentrated acids often make this approach cumbersome and dangerous.[28] Furthermore, the waste management of fluoride ions is a considerable industrial challenge for scalable MXene production.

To overcome the dangers and hazards associated with HF-related etching methods, an alternative synthesis approach that uses molten salts as dry etchants has been reported.[29−33] In 2016, Urbankowski et al. synthesized Ti_4N_3 MXene by a molten salt etching method.[29] Later in 2019, Li et al. synthesized Ti_3C_2 MXene by a molten salt approach using $ZnCl_2$ as a dry etchant.[31] After this work, several Lewis acid salts, such as $CuCl_2$, $CdCl_2$, $CdBr_2$, and SnF_2, were used for molten salt etching of carbide MXenes.[30,33,34]

Although molten salt etching shows promise for safe, scalable, and commercial MXene synthesis, molten salt-etched MXenes are typically not dispersible in water, unlike those synthesized using wet etching methods.[30,31,34] MXenes synthesized by molten salt etching are significantly terminated by halides such as −F, −Cl, and −Br rather than −OH, making the aqueous dispersion of MXene difficult. However, our group recently developed a method to produce water-dispersible Nb_2CT_z MXene nanosheets by using SnF_2 as a dry etchant and then introducing hydroxyl groups to the MXene surface by treating the etched Nb_2CT_z with 0.1 M KOH.[32]

Received: December 6, 2023
Revised: January 10, 2024
Accepted: January 11, 2024
Published: January 24, 2024

The type and number of terminal groups of MXenes are critical for their dispersibility, degradation resistance, and lubrication performance because the terminal groups and their electronegativity have a strong influence on MXene interactions with the surrounding media.[19,26,35,36] However, experimentally controlling terminal groups of MXenes is still challenging, highlighting an important need.

Recent theoretical studies indicate that removal of the MXene terminal groups (such as =O, −Cl, −F, −OH) can be achieved by annealing, but experimental control of surface terminations is still in the developmental stage.[37,38] Hart et al. have computed the effect of removing terminal groups on the electronic properties of several MXene types, with an increase in conductivity after the removal of surface terminations.[38] Later studies suggested that MXene electronic properties can actually shift from semiconducting to metallic when the terminal groups are removed.[39] One possible way to control MXene terminal groups is through thermal annealing. Zhao et al. annealed $Ti_3C_2T_z$ films and showed that this thermal treatment removes hydroxyl groups and creates a passivation or a protective layer of titanium oxide on the thin film surface.[25]

In this work, we demonstrate the control and modification of the surface of molten salt-etched $Ti_3C_2T_z$ via thermal annealing. Here, the annealing step is carried out under argon to minimize the $Ti_3C_2T_z$ oxidation. The molten salt-etched $Ti_3C_2T_z$ possesses significant halide terminations, making it difficult to disperse them in water or other solvents. The much of halide terminations of ML-$Ti_3C_2T_z$ are removed by annealing, and we hypothesize that the removal of terminal groups creates bare sites, which can be further modified. The annealed multilayered (ML) $Ti_3C_2T_z$ (MXene clay) is washed with KOH, and the resulting MXene powder is water-dispersible, which is beneficial in applications such as inks and paints. We hypothesize that washing with KOH allowed to add the hydroxyl groups on the MXene surface. Separately, the annealed ML-$Ti_3C_2T_z$ is treated with 3-aminopropyl triethoxysilane (APTES) and studied using FTIR spectroscopy to show that this approach can be generalized to functional groups beyond −OH. Further, the OH and APTES-functionalized ML-$Ti_3C_2T_z$ are used as a solid lubricant by evaluating their friction performance.

EXPERIMENTAL METHODS AND CHARACTERIZATION

Methods. *Synthesis of Multilayered $Ti_3C_2T_z$.* The Ti_3AlC_2 (purchased from Sigma-Aldrich) phase for $Ti_3C_2T_z$ synthesis was procured from Sigma-Aldrich. 1 g of Ti_3AlC_2 was mixed with 2.28 g of $CuCl_2$ powder (1:3 molar ratio), 0.76 g of KCl, and 0.6 g of NaCl as reported earlier.[34] The mixture was placed in an alumina boat and heated in a tube furnace for 24 h at 750 °C (a ramp rate of 5 °C/min) under argon to carry out the molten salt etching of $Ti_3C_2T_z$. The etched ML-$Ti_3C_2T_z$ was washed in a 0.1 M ammonium persulfate (APS) solution for 2 h to remove Cu and unreacted salt. After APS treatment, the dispersion was centrifuged at 9000 rpm for 10 min to separate APS from ML-$Ti_3C_2T_z$. The ML-$Ti_3C_2T_z$ was then washed with deionized water at 9000 rpm for 15 min four times to wash off any remaining APS.

Annealing of Multilayered $Ti_3C_2T_z$. The multilayered $Ti_3C_2T_z$ was freeze-dried for 36 h to remove excess water before thermal annealing. Then, the dried multilayered $Ti_3C_2T_z$ was placed in an alumina boat and annealed in a tube furnace at 600 °C (a ramp rate of 5 °C/min) under an inert (argon) atmosphere for 3 h.

Surface Modification and Delamination of $Ti_3C_2T_z$. The annealed ML-$Ti_3C_2T_z$ was then treated with 0.1 M KOH for 3 h to add on hydroxyl groups (−OH). After KOH treatment, ML-$Ti_3C_2T_z$ solution was centrifuged at 9000 rpm for 10 min to separate KOH and ML-$Ti_3C_2T_z$. The ML-$Ti_3C_2T_z$ was intercalated with DMSO (1 mL of DMSO per 60 mg of $Ti_3C_2T_z$) for 20 h. The intercalated ML-$Ti_3C_2T_z$ was washed with water 3 times to wash off DMSO and collect the sediment. The obtained sediment was redispersed in deionized water and ultrasonicated in a sealed glass jar for 1 h for delamination. The delaminated $Ti_3C_2T_z$ dispersion was centrifuged at 3500 rpm for 45 min, and the supernatant was collected (delaminated $Ti_3C_2T_z$). The supernatant containing the delaminated $Ti_3C_2T_z$ was freeze-dried for 24 h to conduct further experiments.

APTES-Modified ML-$Ti_3C_2T_z$. 0.1 g of annealed ML-$Ti_3C_2T_z$ powder was immersed in the solution of water and ethanol. The mixture was then ultrasonicated to mix them homogeneously. The APTES solution was dispersed into an MXene dispersion dropwise and then allowed to react for 20 h. Subsequently, the mixture was centrifuged 3 times with the ethanol solution to remove excess APTES, and the sediment was collected and freeze-dried for further characterization. The surface modification of MXene has been tried several times, and sometimes we were not able to modify the surface chemistry, which can be attributed to the bulky APTES molecules.

Characterization. *Scanning Electron Microscopy (SEM).* An FEI Quanta 600 field-emission scanning electron microscope was used to study the morphology of $Ti_3C_2T_z$. The supernatant was collected and freeze-dried to obtain a dry powder. SEM was performed on these dried powder samples using an acceleration voltage of 5−20 kV.

X-ray Diffraction (XRD). XRD was performed on freeze-dried samples (before and after annealed ML-$Ti_3C_2T_z$) using a Bruker D8 powder X-ray diffractometer fitted with a LynxEye detector in a Bragg−Brentano geometry with a CuKa (l = 1.5418 Å) radiation source. A zero-background sample holder was used to test these samples with a scanning rate of 1.5 s per step and a step size of 0.02°.

X-ray Photoelectron Spectroscopy (XPS). An XPS/UPS system with an Argus detector was used for the XPS analysis of the freeze-dried ML-$Ti_3C_2T_z$ samples (before and after annealed MXenes). The sample holder was initially cleaned with isopropyl alcohol, and the samples were placed on the sample holder using a conducting carbon tape. The high-resolution XPS spectra of all of the elements were obtained using a pass energy of 20 eV and a step size of 0.05 eV. The deconvolution spectra of Ti 2p, C 1s, O 1s, and Cl 2p were obtained following the procedure defined by Halim et al.[40] Component fitting was performed using CasaXPS software, and a Shirley-type background function was used to determine the background contribution. The component spectra were calibrated using the carbon peak (C−C, 284.8 eV). Elemental spectra were subsequently separated into the components for $Ti_3C_2T_z$ and listed separately in the graph. There were a few significant constraints while doing the peak fitting; first, all binding energies were allowed to shift in 0.02 eV intervals and were constrained to ±0.5 eV of their initial values. The full-width at half maximum values of components were also constrained. Finally, Ti components in the Ti 2p spectra were fit using asymmetric peaks with high binding energy tails due to their conducting behavior. All peaks and curves were fitted by using Gaussian−Lorentzian curves.

Dynamic Light Scattering (DLS). A Zetasizer Nano ZS90 from Malvern Instruments was used to determine the hydrodynamic diameters of aqueous $Ti_3C_2T_z$ nanosheets at a scattering angle of 90° under ambient conditions. A diluted concentration of 0.05 mg/mL of the aqueous dispersion of $Ti_3C_2T_z$ nanosheets was used for taking the measurements.

ζ Potential Measurement. A Zetasizer Nano ZS90 from Malvern Instruments and a DTS 1070 capillary cell from Malvern Instruments were used to determine the ζ potential of aqueous $Ti_3C_2T_z$ nanosheets under ambient conditions. A diluted concentration of 0.05 mg/mL of the aqueous dispersion of $Ti_3C_2T_z$ nanosheets was used for taking the measurements.

Atomic Force Microscopy (AFM). The freeze-dried $Ti_3C_2T_z$ nanosheet samples were dispersed in water at a concentration of 0.05 mg/mL, bath sonicated for 15 min, and then drop-cast over a silicon wafer. The drop-cast silicon wafer was used to perform AFM using a Bruker Dimension Icon AFM. The height profiles were obtained using a MultiMode scanning probe microscope.

Fourier Transform Infrared (FTIR) Spectroscopy. The surface chemistry of freeze-dried $Ti_3C_2T_z$ was analyzed by using Fourier

https://doi.org/10.1021/acsami.3c18232
ACS Appl. Mater. Interfaces 2024, 16, 6290−6300

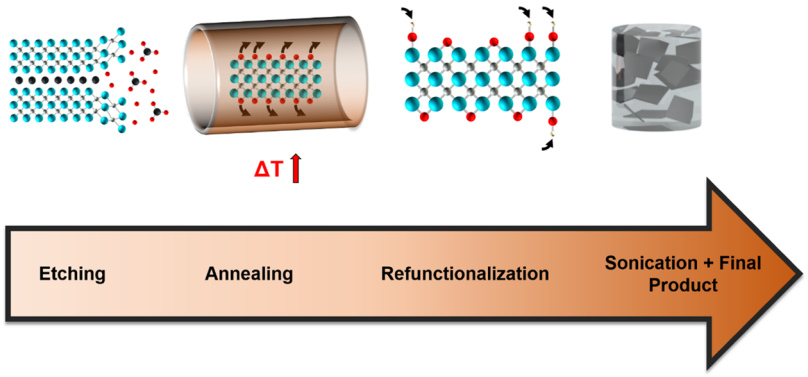

Figure 1. Schematic depicting the steps (molten salt etching, annealing, refunctionalization, and delamination) involved in $Ti_3C_2T_z$ synthesis and surface modification.

transform infrared (FTIR) spectroscopy (Bruker INVENIO R) with a diamond crystal Platinum ATR accessory.

Frictional Measurements. The coefficient of friction was evaluated using a tribometer with a pin-on-disk configuration. It consisted of a rotating disk (steel plate) and a fixed E52 100 steel bearing ball (Ø 6.35 mm). The steel substrates used in this study were washed with ethanol and IPA (50:50). Washed substrates were then vacuum-dried for ~6 h before depositing the ML-$Ti_3C_2T_z$ MXene. ML-$Ti_3C_2T_z$ was dispersed in water (concentration 0.5 mg/mL), bath sonicated for 15 min to obtain uniform dispersion, and about 0.2 mL of dispersion was drop-cast on steel substrates (1 cm × 1 cm). The steel substrates were then vacuum-dried to form a solid lubricant film of $Ti_3C_2T_z$.

Thermal Measurements. The Q600 (TA Instruments) was used to measure the weight change (TGA) and true differential heat flow (DSC) in a nitrogen atmosphere using aluminum crucibles with a sealed lid. Approximately 5−10 mg of the ML-$Ti_3C_2T_z$ powder was used for testing. The MXene powder was heated from room temperature to 800 °C.

RESULTS AND DISCUSSION

Figure 1 shows a schematic of the processing steps in the synthesis and surface modification of $Ti_3C_2T_z$. The molten salt etching of Ti_3AlC_2 was conducted using a mixture of $CuCl_2$, KCl, and NaCl as a dry etchant at 750 °C for 24 h under an argon flow to obtain ML-$Ti_3C_2T_z$.[34] This method was selected because of its ability to produce multilayered MXenes with minimal impurities and reasonable control over obtaining Cl-terminated $Ti_3C_2T_z$.[34] The molten salt-etched $Ti_3C_2T_z$ was treated with 0.1 M ammonium persulfate (APS) solution to remove copper impurities and then washed with water to remove traces of APS from MXenes. The yield (MAX to MXene conversion) was calculated based on the solids after APS washing (removal of Cu impurities) and found to be ~58%. The ML-$Ti_3C_2T_z$ was further annealed in a tube furnace at 600 °C and then treated with 0.1 M KOH solution to add −OH groups on available bare sites. The ML-$Ti_3C_2T_z$ was intercalated with DMSO and then delaminated by bath sonication to obtain a $Ti_3C_2T_z$ nanosheet dispersion.

TGA-DSC analysis of ML-$Ti_3C_2T_z$ (Figure 2) was conducted from room temperature to 800 °C in an inert N_2 atmosphere. The endothermic peak observed in the DSC curve at 570 °C and weight loss of about 5% in the temperature range of 400−600 °C were attributed to the loss of surface functional groups of $Ti_3C_2T_z$.

The morphology of molten salt-etched ML-$Ti_3C_2T_z$ was analyzed using scanning electron microscopy (SEM), as shown in Figure 3. The layered structure typical of the Ti_3AlC_2 phase precursor used in the synthesis is demonstrated in Figure 3a.

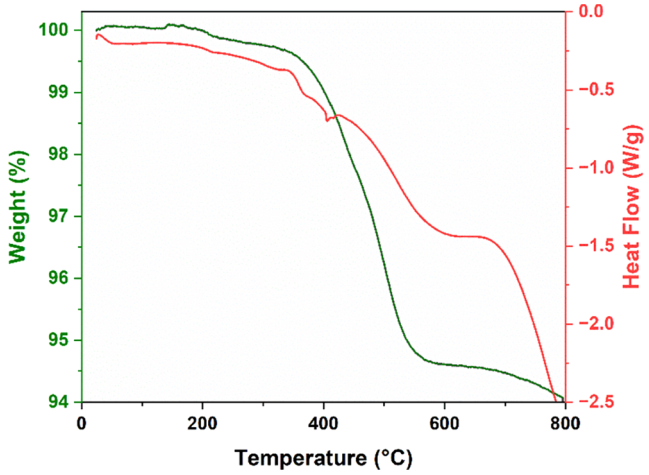

Figure 2. TGA-DSC analysis on ML-$Ti_3C_2T_z$ indicates the thermal stability of MXenes.

The etching of $Ti_3C_2T_z$ at 750 °C resulted in a typical accordion structure of stacked MXene layers, as demonstrated in Figure 3b. The resulting accordion-like structure (Figure 3b) and elemental composition (Table 1) confirm the successful removal of Al from the Ti_3AlC_2 phase.[41] Even after annealing at 600 °C for 3 h under argon, ML-$Ti_3C_2T_z$ exhibits an accordion-like structure and no sign of degradation (Figure 3c), indicating thermal stability.[25]

XRD analysis (Figure 3d) was further utilized to confirm the synthesis of $Ti_3C_2T_z$. The (002) peak (ML-$Ti_3C_2T_z$ after APS washed) at 7.7° indicates the successful removal of Al and formation of $Ti_3C_2T_z$ after etching. Further, the effect of APS washing and annealing was evaluated by XRD. The APS treatment is used to remove Cu impurities, which was confirmed by the disappearance of the 49° peak, as shown in Figure 3d.[34] The only unusual feature that we observed in the XRD was the shift of the 002 peak of delaminated MXene to the right rather than the left. Verger et al. found that *d*-spacing can decrease even after intercalation and delamination, possibly due to the residual solvent between the layers.[42] A similar behavior was observed by Kotasthane et al. in the case of V_2CT_z MXene.[43] The annealing of $Ti_3C_2T_z$ shifted the (002) peak of $Ti_3C_2T_z$ from 7.7 to 7.9°, indicating the change of *d*-spacing between the layers of $Ti_3C_2T_z$.[38] The reduction in the *d*-spacing of $Ti_3C_2T_z$ can be attributed to the decrease of the in-plane strain imposed on the titanium carbide lattice due to the removal of terminal groups of MXenes.[30] The additional peaks (008) and (104) are attributed

https://doi.org/10.1021/acsami.3c18232
ACS Appl. Mater. Interfaces 2024, 16, 6290−6300

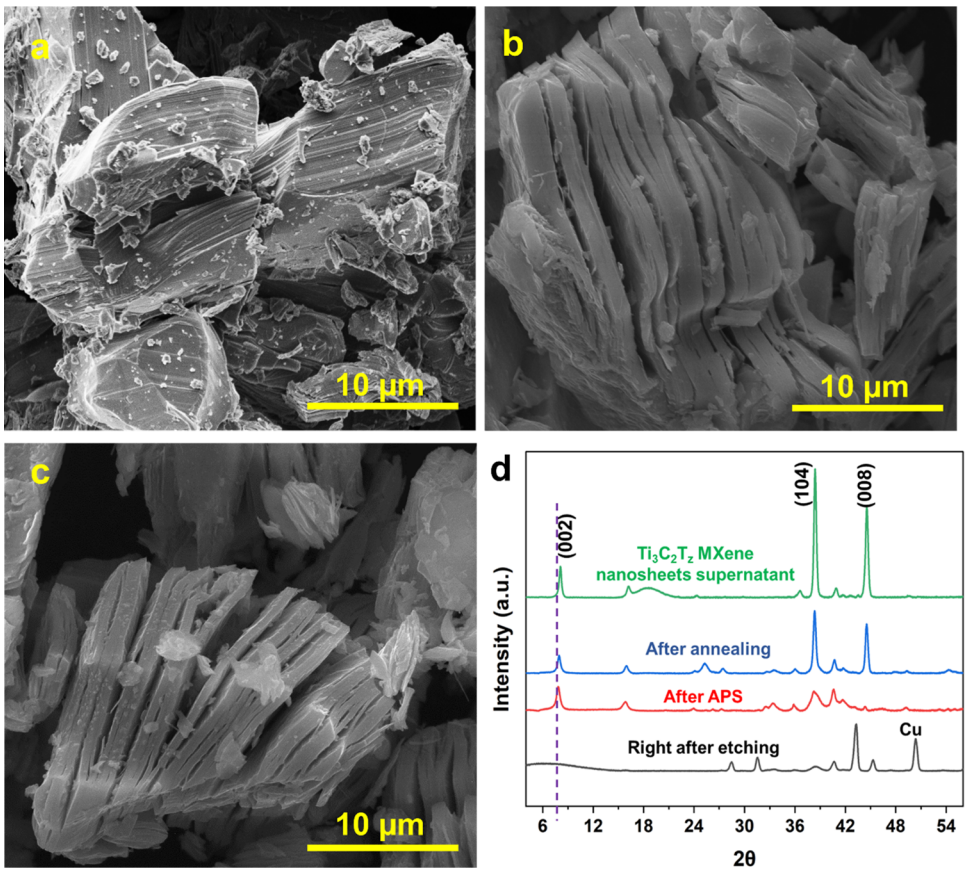

Figure 3. Morphology of the MAX phase and $Ti_3C_2T_z$: SEM of (a) precursor Ti_3AlC_2 and (b) ML-$Ti_3C_2T_z$ after etching; (c) ML-$Ti_3C_2T_z$ after annealing at 600 °C for 3 h; and (d) XRD analysis of ML-$Ti_3C_2T_z$ after APS washing, annealing, and delaminated nanosheets.

Table 1. Elemental Composition of ML-$Ti_3C_2T_z$ (before and after Annealing) Obtained by SEM-EDS

elements	ML-$Ti_3C_2T_z$ before annealing wt %	ML-$Ti_3C_2T_z$ after annealing wt %
Ti	50.5 ± 3.4	57 ± 4.1
C	20.2 ± 2.6	23 ± 1.9
Cl	18 ± 1.6	10.2 ± 2.8
O	10.8 ± 2.3	8.9 ± 1.4
Cu	0.3 ± 0.2	0.8 ± 0.5
Al	0.3 ± 0.2	0.1 ± 0.1

to the formation of TiC during the annealing and processing of MXenes.[44]

The elemental composition of $Ti_3C_2T_z$ before and after annealing was examined by SEM-EDS, as shown in Table 1 and Figure 4. Table 1 confirms the presence of typical elements of $Ti_3C_2T_z$, including Ti, C, O, and Cl, and other elements, such as Cu and Al. The presence of Al can be attributed to the existence of some unetched Ti_3AlC_2 phase, and the appearance of Cu can be ascribed to a small amount of leftover Cu impurities in ML-$Ti_3C_2T_z$ even after APS treatment. The slight increase of the Cu fraction after thermal annealing is likely due to a heat-induced

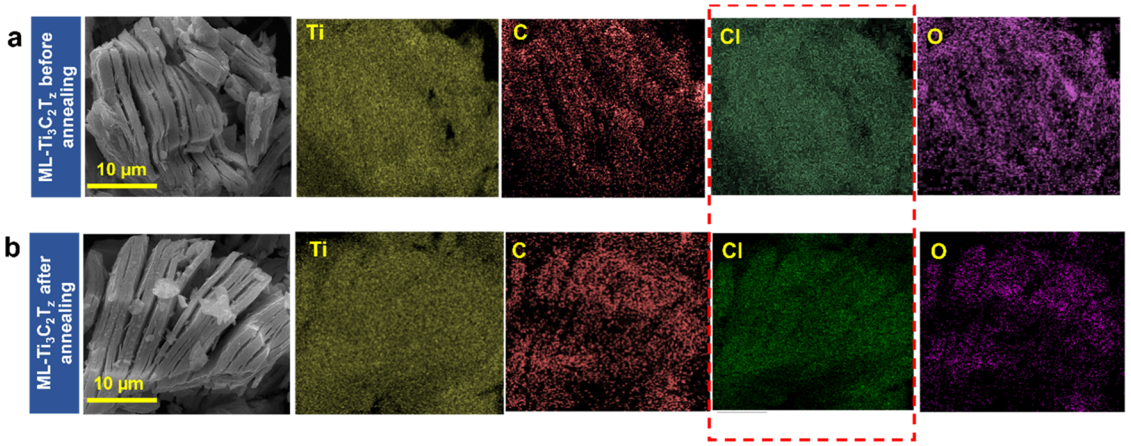

Figure 4. EDS mapping of ML-$Ti_3C_2T_z$: (a) before annealing; (b) after annealing at 600 °C for 3 h under argon.

https://doi.org/10.1021/acsami.3c18232
ACS Appl. Mater. Interfaces 2024, 16, 6290−6300

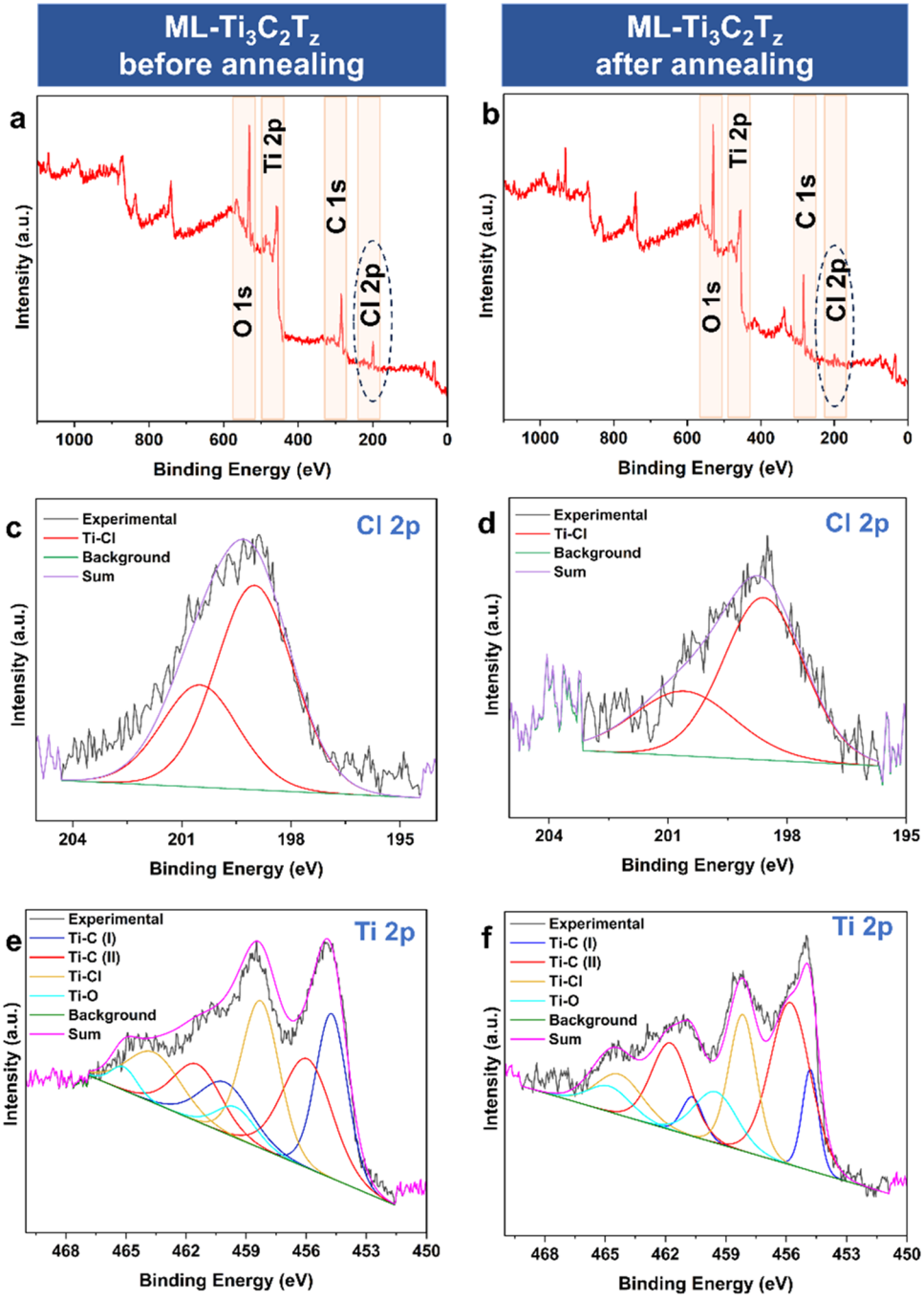

Figure 5. XPS survey spectra of ML-$Ti_3C_2T_z$: (a) before annealing; (b) after annealing. Deconvoluted spectra of ML-$Ti_3C_2T_z$: (c) Cl 2p before annealing, (d) Cl 2p after annealing, (e) Ti 2p before annealing, and (f) Ti 2p after annealing.

migration of Cu impurities from the interior to the exterior of ML-$Ti_3C_2T_z$. The loss of wt % of oxygen after thermal annealing can be attributed to the evaporation of free intercalated water from the ML-$Ti_3C_2T_z$ layers. The thermally annealed ML-$Ti_3C_2T_z$ also showed the presence of typical elements Ti, C, O, and Cl; however, the Cl content was reduced from 18.0 wt % (before annealing) to 10.2 wt % (after annealing). The decrease in chlorine content after annealing was attributed to the removal of much of the −Cl surface terminations from $Ti_3C_2T_z$. EDS mapping (Figure 4) of ML-$Ti_3C_2T_z$ before and after annealing showed uniform distributions of Ti, C, Cl, and O. The reduced chlorine content after annealing can also be observed in the EDS map, which shows a drop in the distribution of Cl on ML-$Ti_3C_2T_z$.

XPS analysis was performed to confirm the removal of many of the surface terminations of ML-$Ti_3C_2T_z$, as shown in Figures 5, S1, and S2. The survey spectra of as-prepared $Ti_3C_2T_z$ (Figure 5a) confirmed the presence of typical elements: Ti, C, O, and Cl of ML-$Ti_3C_2T_z$, which is in accordance with the EDS data examined earlier. The XPS analysis (Figure 5a,b and Table 2) also indicated a drop in the concentration of Cl 2p from 6.3 to 3.4 atom % after annealing. This change in concentration is a result of the removal of many −Cl terminations from $Ti_3C_2T_z$. The deconvoluted Cl 2p spectra shown in Figure 5c,d also show the change in chlorine after annealing. The deconvoluted Ti 2p

https://doi.org/10.1021/acsami.3c18232
ACS Appl. Mater. Interfaces 2024, 16, 6290−6300

Table 2. Elemental Composition Obtained by XPS for ML-$Ti_3C_2T_z$ before and after Annealing

elements	ML-$Ti_3C_2T_z$ before annealing atom %	ML-$Ti_3C_2T_z$ after annealing atom %	delaminated $Ti_3C_2T_z$ nanosheets atom %
Ti 2p	18.5 ± 1.7	17.9 ± 1.2	17.3 ± 1.5
Cl 2p	6.3 ± 1.1	3.4 ± 0.9	1.1 ± 0.7
C 1s	50.5 ± 4.7	52.3 ± 2.7	48.4 ± 1.9
O 1s	24.7 ± 1.8	25.1 ± 2.1	31.7 ± 3.9
Cu 2p		1.3 ± 0.2	1.5 ± 0.3

spectra (Figure 5e,f) of ML-$Ti_3C_2T_z$ before and after annealing showed a drop in the Ti−Cl content by 34.5 atom %, confirming the partial removal of much of −Cl from the ML-$Ti_3C_2T_z$ surface. The removal of much of −Cl species from the surface may create bare sites for further surface modification; we evaluate this possibility below.[45]

The slight variation in the overall elemental composition obtained from EDS and XPS is due to their different detection ranges. XPS is more sensitive of the two techniques. However, both analysis techniques showed a similar trend: a decrease in chlorine fraction after thermal annealing.

The annealed ML-$Ti_3C_2T_z$ was treated with 0.1 M KOH solution to reintroduce hydroxyl groups following the procedure reported earlier by our group.[33] This was followed by intercalation by DMSO, and then delaminated $Ti_3C_2T_z$ nanosheets were produced by bath sonication. The $Ti_3C_2T_z$ dispersion was evaluated by measuring the zeta potential (ζ) and the hydrodynamic diameter. The data indicate a ζ potential (Figure 6a) of −34.8 mV, which confirms the colloidal stability of delaminated $Ti_3C_2T_z$ nanosheets.[46−48] This colloidal stability can be attributed to the addition of the −OH group to the delaminated $Ti_3C_2T_z$ surface. The DLS measurements (Figure 6b) revealed that delaminated $Ti_3C_2T_z$ exhibited a hydrodynamic diameter of 728 nm. However, the appearance of a small peak at 5360 nm might be due to ML-$Ti_3C_2T_z$ in the final supernatant. The morphology of delaminated $Ti_3C_2T_z$ was then studied under SEM (Figure 6c) and AFM (Figure 6d). SEM confirms the sheetlike morphology of delaminated $Ti_3C_2T_z$ nanosheets. The AFM analysis of the obtained dispersion of delaminated $Ti_3C_2T_z$ nanosheets showed thickness (Figures 6d and S3) ranging from 1.5 to 2 nm, confirming the presence of a few-layer $Ti_3C_2T_z$.[5,9,46]

The addition of −OH groups on the annealed ML-$Ti_3C_2T_z$ was further confirmed by the FTIR spectra shown in Figure 7a. The FTIR peak at 3334 cm^{-1} can be attributed to the stretching vibrations of −OH, confirming the addition of the −OH group to delaminated $Ti_3C_2T_z$.[49] The XPS analysis (Figures 7b,c and S4) was performed on vacuum-filtered $Ti_3C_2T_z$ papers formed from the supernatant to analyze the surface terminations of delaminated nanosheets. The survey spectra of KOH-treated MXene (Figure 7b) exhibited higher atom % of the O 1s compared to annealed $Ti_3C_2T_z$ (Table 2), indicating the addition of −OH groups to the delaminated $Ti_3C_2T_z$ by KOH treatment. The deconvoluted Cl 2p spectra shown in Figure 7c exhibit a small amount (1.06 atom %) of chlorine. The delaminated $Ti_3C_2T_z$ nanosheets confirm the uniform distribution (Figure 7d and Table S1) of Ti, C, Cl, and O.

To demonstrate that this refunctionalization scheme can be generalized to other functional groups, annealed ML-$Ti_3C_2T_z$ was treated with APTES in a mixture of ethanol and water at room temperature for 20 h. FTIR spectroscopy on the APTES-

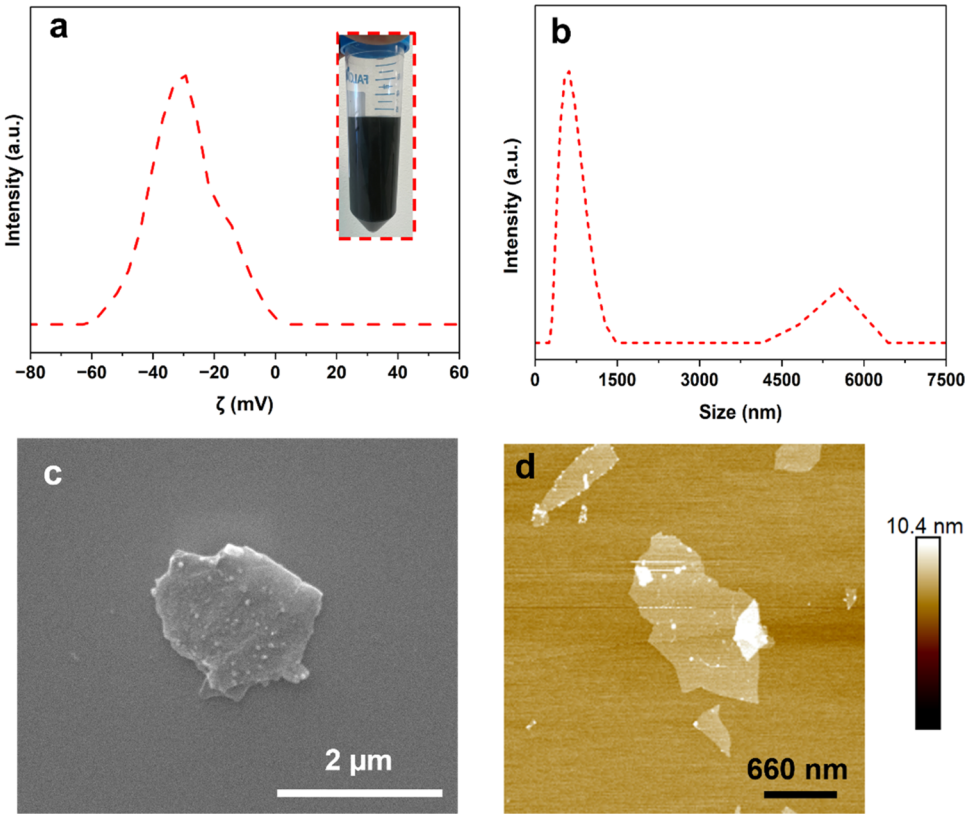

Figure 6. Analysis of delaminated $Ti_3C_2T_z$ nanosheets confirming the formation of stable colloidal solution: (a) zeta potential (ζ); (b) DLS. Nanosheet morphology: (c) SEM and (d) AFM.

https://doi.org/10.1021/acsami.3c18232
ACS Appl. Mater. Interfaces 2024, 16, 6290−6300

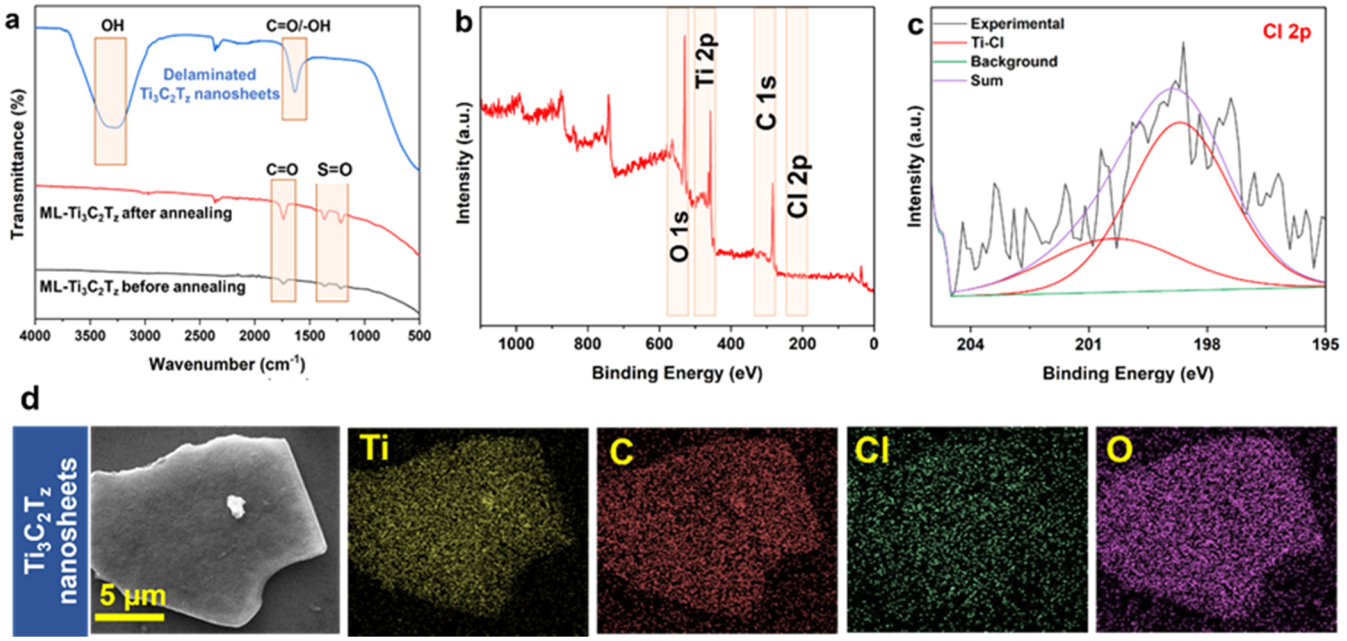

Figure 7. Delaminated $Ti_3C_2T_z$ nanosheets: (a) FTIR showing the addition of hydroxyl groups, (b) survey spectra, (c) deconvoluted Cl 2p spectra, and (d) SEM-EDS mapping of delaminated $Ti_3C_2T_z$ nanosheets.

modified ML-$Ti_3C_2T_z$ (Figure 8) revealed three new peaks at 3249, 2921, and 1634 cm^{-1}, respectively, that appeared after the

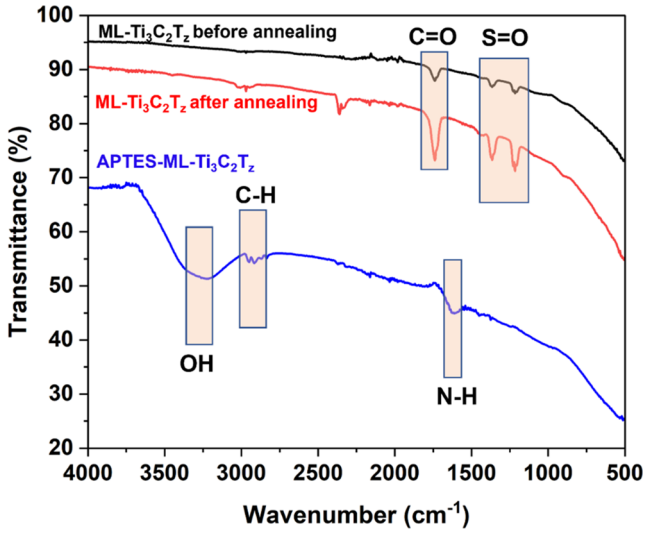

Figure 8. FTIR spectra of ML-$Ti_3C_2T_z$ before annealing, after annealing, and after APTES treatment.

treatment. The peak at 2921 cm^{-1} is attributed to symmetric and asymmetric vibrations of CH bonds in the alkyl chain of APTES.[50] Moreover, the peak highlighted at around 1634 cm^{-1} can be ascribed to the bending mode of the -NH bond of the primary amine.[51] The broad peak around at 3249 cm^{-1} originates from the −OH surface terminations.[52] Collectively, these data indicate that refunctionalization with APTES was successful.

The weak interlayer interaction, low shear resistance, ease of formation of a tribo-layer, and self-lubricating ability make MXenes outstanding candidates for solid lubrication.[53,54] In this work, we focused on the multilayered-$Ti_3C_2T_z$ MXene only because multilayered MXenes have higher load-bearing capacity and easy-to-shear ability than single-layered sheets.[53,55] The −OH and APTES surface-modified ML-$Ti_3C_2T_z$ were utilized as a solid lubricant and evaluated for their tribological properties after surface modifications. The APTES-ML-$Ti_3C_2T_z$ and OH-ML-$Ti_3C_2T_z$ MXene dispersions are stable for 3−5 days. The solid lubricant coatings evaluated in this work are prepared from fresh dispersions prior to any settling, which resulted in fairly uniform coatings as shown in Figure S5 and Table S2. The lubrication performance of nonannealed (before annealing or as prepared) and after annealing of ML-$Ti_3C_2T_z$ was evaluated under a load of 1.0 N, and it exhibited an average coefficient of friction (COF) of 0.26 and 0.42, respectively (Figure 9), indicating that annealing alone does not improve the perform-

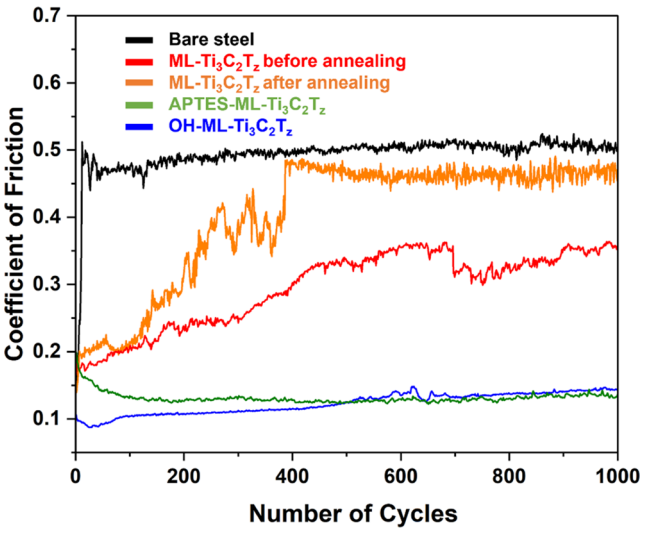

Figure 9. Tribological performance of the bare steel substrate, nonannealed and annealed ML-$Ti_3C_2T_z$-coated substrate, APTES-modified ML-$Ti_3C_2T_z$-coated substrate, and OH-modified ML-$Ti_3C_2T_z$ substrate.

https://doi.org/10.1021/acsami.3c18232
ACS Appl. Mater. Interfaces 2024, 16, 6290−6300

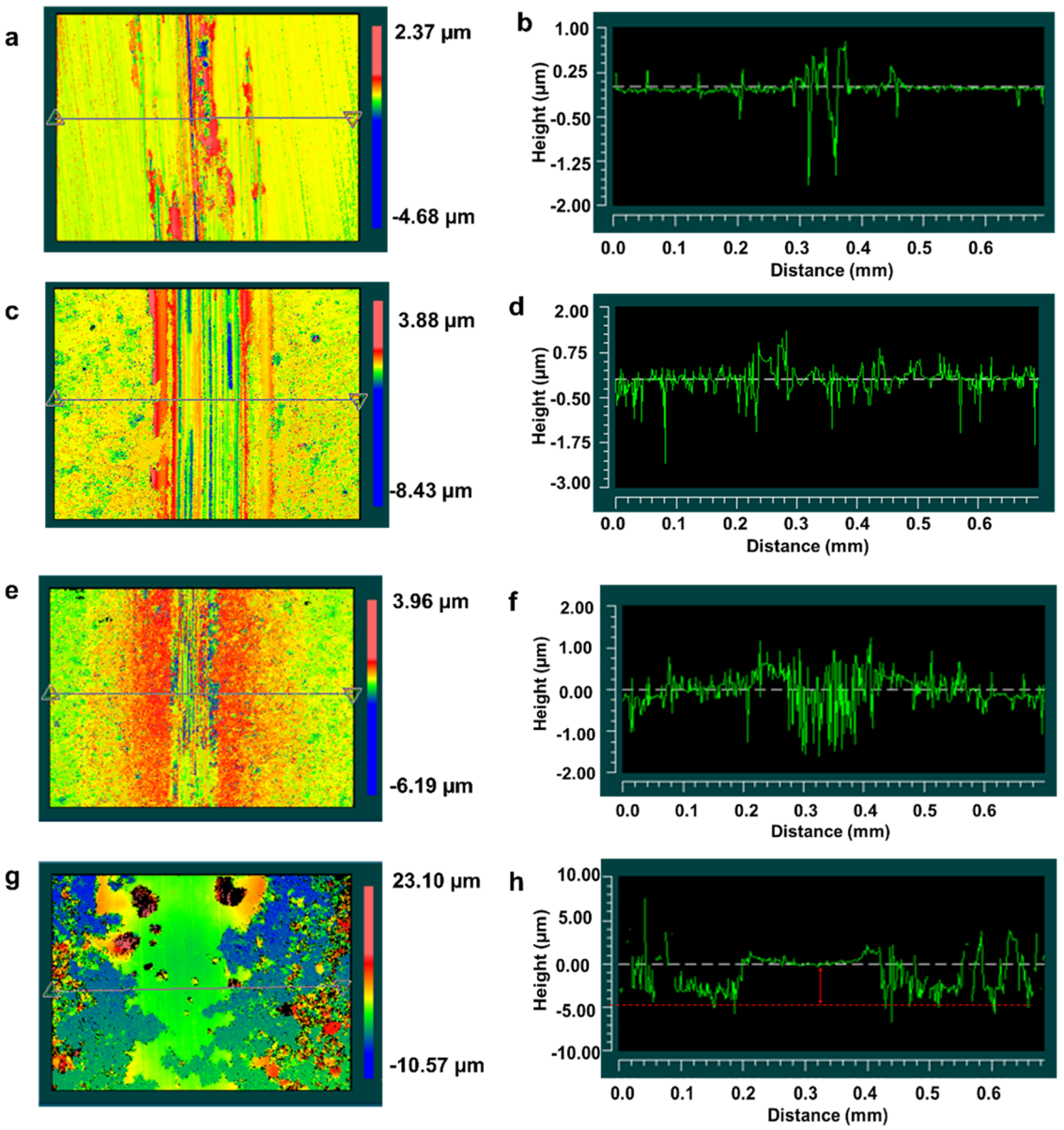

Figure 10. White light interferometry (WLI) images and corresponding height profile across the wear track for (a, b) bare steel substrate, (c, d) nonannealed ML-$Ti_3C_2T_z$ substrate, (e, f) OH-modified ML-$Ti_3C_2T_z$ substrate, and (g, h) APTES-modified ML-$Ti_3C_2T_z$ substrate. (All of the WLI data were recorded on the steel substrate after the tribotest).

ance. The increase of COF after initial few cycles can be attributed to the poor adhesion of ML-$Ti_3C_2T_z$ which resulted into a crashed or pushed out of the substrate allowing the metal-to-metal friction. The surface-modified $Ti_3C_2T_z$ was successfully drop-cast on the steel substrate and dried under a vacuum before taking measurements. However, the OH and APTES-modified ML-$Ti_3C_2T_z$ showed an average coefficient of friction (COF) of 0.14 and 0.16, respectively, at a normal load of 1.0 N, significantly reduced compared to bare steel disks or ML-$Ti_3C_2T_z$ without annealing and any surface modification. According to the literature, the MILD method synthesized $Ti_3C_2T_z$ possesses an average COF in the range 0.2−0.5.[19,53,56,57] The OH and APTES-modified $Ti_3C_2T_z$ exhibited a reduction in COF by 70.1 and 66.7%, respectively, when compared with bare steel substrates. The reduction in friction after surface modification can be attributed to the increase of adhesion of $Ti_3C_2T_z$ to the substrate, which ultimately generated the tribofilm on the substrate. The interaction of terminal groups of MXene does play a vital role in deciding the frictional performance and durability of the coating, as reported by Parra-Muñoz et al.[19] The presence of −OH terminal groups on MXene can improve the lubrication properties by adsorbing water molecules and creating a boundary layer that reduces friction and wears.[58] In the case of APTES molecules, the amino groups can form hydrogen bonds with water molecules, creating a boundary layer that can act as a lubricant.[59]

The success of the solid lubricant as coatings can be evaluated based on low coefficient friction over many mechanical cycles. This performance greatly depends on the coating uniformity and the coating/substrate adhesion.[60,61] The interferometry images of the steel substrate (after tribo-testing) without any lubricant (Figure 10a,b) and the nonannealed ML-$Ti_3C_2T_z$-coated steel substrate (Figure 10c,d) demonstrated the deep scratches or grooves due to substrate wear during the tribo-testing. Also, the

https://doi.org/10.1021/acsami.3c18232
ACS Appl. Mater. Interfaces 2024, 16, 6290−6300

nonannealed ML-$Ti_3C_2T_z$-coated steel substrate showed deep grooves. The low value of COF of OH and APTES-modified ML-$Ti_3C_2T_z$ can be attributed to the formation of a tribofilm.[17,19,53−55,58,62,63] This formation of MXene tribofilm is consistent with the earlier reports on $Ti_3C_2T_z$ tribology.[54,58,62] The APTES-modified ML-$Ti_3C_2T_z$ exhibited better tribological behavior than OH-modified MXene because adding APTES can enhance surface adhesion and improve the load-bearing capacity and durability of tribological systems.[59] The amino groups on the APTES-modified ML-$Ti_3C_2T_z$ can adhere to the metal surface, creating a strong interface.[19] The higher height values on the wear track indicate the formation of the MXene tribofilm developed while tribo-testing. This formation of MXene tribofilm is in accordance with the earlier reports of $Ti_3C_2T_z$ tribology.[53,57]

The APTES-modified ML-$Ti_3C_2T_z$ exhibited better tribological behavior than the OH-modified MXene because adding APTES can enhance surface adhesion and improve the load-bearing capacity and durability of tribological systems.[59] The amino groups on the APTES-modified ML-$Ti_3C_2T_z$ can form better adhesion with the metal surface, creating a strong interface.

CONCLUSIONS

In conclusion, the thermal annealing approach was used to control the surface terminations of molten salt-etched $Ti_3C_2T_z$. Thermal annealing at 600 °C under argon was able to remove much of the −Cl terminations of $Ti_3C_2T_z$. Here, we showed that removing much of the −Cl surface terminations from $Ti_3C_2T_z$ created bare sites for further modification of the MXenes. Refunctionalization of the annealed $Ti_3C_2T_z$ surface on produced bare sites was carried out using −OH and APTES. The obtained $Ti_3C_2T_z$ was confirmed using SEM-EDS, XPS, and FTIR spectral analyses. Furthermore, the annealed and refunctionalized $Ti_3C_2T_z$ showed promise as a solid lubricant for tribological application with a 65−70% reduction in the coefficient of friction. The thermal annealing method described in this study holds promise for the control of MXene surface functionalization, allowing the tuning of MXene chemistry for desired application-specific property optimization.

ASSOCIATED CONTENT

Supporting Information

The Supporting Information is available free of charge at https://pubs.acs.org/doi/10.1021/acsami.3c18232.

Figure S1: Deconvoluted X-ray photoelectron spectroscopy (XPS) spectra of ML-$Ti_3C_2T_z$ before annealing: (a) C 1s; (b) O 1s; and (c) Cu 2p. Figure S2: Deconvoluted X-ray photoelectron spectroscopy (XPS) spectra of ML-$Ti_3C_2T_z$ after annealing: (a) C 1s; (b) O 1s; and (c) Cu 2p. Figure S3: The corresponding (to Figure 6d) height profile of delaminated $Ti_3C_2T_z$ nanosheets obtained by atomic force microscopy (AFM). Figure S4: Deconvoluted X-ray photoelectron spectroscopy (XPS) spectra of delaminated $Ti_3C_2T_z$: (a) C 1s; (b) O 1s; and (c) Cu 2p. Table S1: Elemental composition of delaminated $Ti_3C_2T_z$ nanosheets obtained from SEM-EDS analysis. Figure S5: Surface morphology (SEM) of steel substrates coated with (a) ML-$Ti_3C_2T_z$ before annealing; (b) ML-$Ti_3C_2T_z$ after annealing; (c) OH-ML-$Ti_3C_2T_z$; and (d) APTES-ML-$Ti_3C_2T_z$. Table S2: Thickness and roughness of the ML-$Ti_3C_2T_z$ MXene-coated substrates (PDF)

AUTHOR INFORMATION

Corresponding Author

Micah J. Green − *Department of Materials Science and Engineering, Texas A&M University, College Station, Texas 77843, United States; Artie McFerrin Department of Chemical Engineering, Texas A&M University, College Station, Texas 77843, United States;* orcid.org/0000-0001-5691-0861; Email: micah.green@tamu.edu

Authors

Kailash Arole − *Department of Materials Science and Engineering, Texas A&M University, College Station, Texas 77843, United States; Artie McFerrin Department of Chemical Engineering, Texas A&M University, College Station, Texas 77843, United States;* orcid.org/0000-0002-4516-889X

Stefano A. Micci-Barreca − *Artie McFerrin Department of Chemical Engineering, Texas A&M University, College Station, Texas 77843, United States*

Swarnima Athavale − *Artie McFerrin Department of Chemical Engineering, Texas A&M University, College Station, Texas 77843, United States;* orcid.org/0000-0002-8948-1263

Mohsen Tajedini − *J. Mike Walker '66 Department of Mechanical Engineering, Texas A&M University, College Station, Texas 778843, United States*

Greeshma Raghuvaran − *Department of Materials Science and Engineering, Texas A&M University, College Station, Texas 77843, United States*

Jodie L. Lutkenhaus − *Department of Materials Science and Engineering, Texas A&M University, College Station, Texas 77843, United States; Artie McFerrin Department of Chemical Engineering, Texas A&M University, College Station, Texas 77843, United States;* orcid.org/0000-0002-2613-6016

Miladin Radovic − *Department of Materials Science and Engineering, Texas A&M University, College Station, Texas 77843, United States;* orcid.org/0000-0003-4571-2848

Hong Liang − *Department of Materials Science and Engineering, Texas A&M University, College Station, Texas 77843, United States; J. Mike Walker '66 Department of Mechanical Engineering, Texas A&M University, College Station, Texas 778843, United States;* orcid.org/0000-0001-9015-3358

Complete contact information is available at: https://pubs.acs.org/10.1021/acsami.3c18232

Notes

The authors declare no competing financial interest.

ACKNOWLEDGMENTS

The authors acknowledge the use of the TAMU Materials Characterization Facility (RRID: SCR_022202) and the Microscopy & Imaging Center (RRID: SCR_022128). They acknowledge support from the National Science Foundation, award CMMI 2240554. They also acknowledge Dr. Mustafa Akbulut of TAMU for access to the ZetaSizer instrument for zeta potential and dynamic light scattering measurements, and Dr. Emily Pentzer of TAMU for FTIR spectroscopy access.

REFERENCES

(1) Naguib, M.; Kurtoglu, M.; Presser, V.; Lu, J.; Niu, J.; Heon, M.; Hultman, L.; Gogotsi, Y.; Barsoum, M. W. Two-Dimensional Nanocrystals Produced by Exfoliation of Ti3alc2. *Adv. Mater.* **2011**, *23* (37), 4248−4253.

(2) Gogotsi, Y.; Anasori, B. *The Rise of Mxenes*; ACS Publications, 2019.
(3) Yang, W.; Yang, J.; Byun, J. J.; Moissinac, F. P.; Xu, J.; Haigh, S. J.; Domingos, M.; Bissett, M. A.; Dryfe, R. A.; Barg, S. 3d Printing of Freestanding Mxene Architectures for Current-Collector-Free Supercapacitors. *Adv. Mater.* **2019**, *31* (37), No. 1902725.
(4) Naguib, M.; Mochalin, V. N.; Barsoum, M. W.; Gogotsi, Y. 25th Anniversary Article: Mxenes: A New Family of Two-Dimensional Materials. *Adv. Mater.* **2014**, *26* (7), 992−1005.
(5) Magnuson, M.; Halim, J.; Näslund, L.-Å. Chemical Bonding in Carbide Mxene Nanosheets. *J. Electron Spectrosc. Relat. Phenom.* **2018**, *224*, 27−32.
(6) Shahzad, F.; Alhabeb, M.; Hatter, C. B.; Anasori, B.; Hong, S. M.; Koo, C. M.; Gogotsi, Y. Electromagnetic Interference Shielding with 2d Transition Metal Carbides (Mxenes). *Science* **2016**, *353* (6304), 1137−1140.
(7) Zhang, C. J.; McKeon, L.; Kremer, M. P.; Park, S.-H.; Ronan, O.; Seral-Ascaso, A.; Barwich, S.; Coileáin, C. Ó.; McEvoy, N.; Nerl, H. C.; et al. Additive-Free Mxene Inks and Direct Printing of Micro-Supercapacitors. *Nat. Commun.* **2019**, *10* (1), No. 1795.
(8) Hu, G.; Kang, J.; Ng, L. W.; Zhu, X.; Howe, R. C.; Jones, C. G.; Hersam, M. C.; Hasan, T. Functional Inks and Printing of Two-Dimensional Materials. *Chem. Soc. Rev.* **2018**, *47* (9), 3265−3300.
(9) Tezel, G. B.; Arole, K.; Holta, D. E.; Radovic, M.; Green, M. J. Interparticle Interactions and Rheological Signatures of Ti3c2tz Mxene Dispersions. *J. Colloid Interface Sci.* **2022**, *605*, 120−128.
(10) Saha, S.; Arole, K.; Radovic, M.; Lutkenhaus, J. L.; Green, M. J. One-Step Hydrothermal Synthesis of Porous Ti3c2tz Mxene/Rgo Gels for Supercapacitor Applications. *Nanoscale* **2021**, *13*, 16543.
(11) Jin, Y.; Fan, Y.; Meng, X.; Zhang, W.; Meng, B.; Yang, N.; Liu, S. Theoretical and Experimental Insights into the Mechanism for Gas Separation through Nanochannels in 2d Laminar Mxene Membranes. *Processes* **2019**, *7* (10), 751.
(12) Sarang, K.; Zhao, X.; Holta, D.; Cao, H.; Arole, K.; Flouda, P.; Oh, E.-S.; Radovic, M.; Green, M. J.; Lutkenhaus, J. L. Carbon Additive-Free Crumpled Ti3c2t X Mxene-Encapsulated Silicon Nanoparticle Anodes for Lithium-Ion Batteries. *ACS Appl. Energy Mater.* **2021**, *4* (10), 10762−10773.
(13) Dadashi Firouzjaei, M.; Karimiziarani, M.; Moradkhani, H.; Elliott, M.; Anasori, B. Mxenes: The Two-Dimensional Influencers. *Elsevier* **2022**, *13*, No. 100202.
(14) Zhang, Y.-Z.; El-Demellawi, J. K.; Jiang, Q.; Ge, G.; Liang, H.; Lee, K.; Dong, X.; Alshareef, H. N. Mxene Hydrogels: Fundamentals and Applications. *Chem. Soc. Rev.* **2020**, *49*, 7229−7251, DOI: 10.1039/D0CS00022A.
(15) Bayram, V.; Ghidiu, M.; Byun, J. J.; Rawson, S. D.; Yang, P.; Mcdonald, S. A.; Lindley, M.; Fairclough, S.; Haigh, S. J.; Withers, P. J.; et al. Mxene Tunable Lamellae Architectures for Supercapacitor Electrodes. *ACS Appl. Energy Mater.* **2020**, *3* (1), 411−422.
(16) Tang, X.; Zhou, D.; Li, P.; Guo, X.; Sun, B.; Liu, H.; Yan, K.; Gogotsi, Y.; Wang, G. Mxene-Based Dendrite-Free Potassium Metal Batteries. *Adv. Mater.* **2020**, *32* (4), No. 1906739.
(17) Arole, K.; Tajedini, M.; Sarmah, A.; Athavale, S.; Green, M. J.; Liang, H. Effects of Ti3c2tz Mxene Nanoparticle Additive on Fluidic Properties and Tribological Performance. *J. Mol. Liq.* **2023**, *386*, No. 122435.
(18) Zhang, T.; Chang, L.; Zhang, X.; Wan, H.; Liu, N.; Zhou, L.; Xiao, X. Simultaneously Tuning Interlayer Spacing and Termination of Mxenes by Lewis-Basic Halides. *Nat. Commun.* **2022**, *13* (1), No. 6731.
(19) Parra-Muñoz, N.; Soler, M.; Rosenkranz, A. Covalent Functionalization of Mxenes for Tribological Purposes-a Critical Review. *Adv. Colloid Interface Sci.* **2022**, *309*, No. 102792.
(20) Tang, Q.; Zhou, Z.; Shen, P. Are Mxenes Promising Anode Materials for Li Ion Batteries? Computational Studies on Electronic Properties and Li Storage Capability of Ti3c2 and Ti3c2 × 2 (X= F, Oh) Monolayer. *J. Am. Chem. Soc.* **2012**, *134* (40), 16909−16916.
(21) Peng, C.; Wei, P.; Chen, X.; Zhang, Y.; Zhu, F.; Cao, Y.; Wang, H.; Yu, H.; Peng, F. A Hydrothermal Etching Route to Synthesis of 2d Mxene (Ti3c2, Nb2c): Enhanced Exfoliation and Improved Adsorption Performance. *Ceram. Int.* **2018**, *44* (15), 18886−18893.
(22) Zhang, X.; Liu, Y.; Dong, S.; Yang, J.; Liu, X. Surface Modified Mxene Film as Flexible Electrode with Ultrahigh Volumetric Capacitance. *Electrochim. Acta* **2019**, *294*, 233−239.
(23) Eklund, P.; Rosen, J.; Persson, P. O. Å. Layered Ternary M N+ 1ax N Phases and Their 2d Derivative Mxene: An Overview from a Thin-Film Perspective. *J. Phys. D: Appl. Phys.* **2017**, *50* (11), No. 113001.
(24) Athavale, S.; Micci-Barreca, S.; Arole, K.; Kotasthane, V.; Blivin, J.; Cao, H.; Lutkenhaus, J. L.; Radovic, M.; Green, M. J. Advances in the Chemical Stabilization of Mxenes. *Langmuir* **2023**, *39*, 918−928, DOI: 10.1021/acs.langmuir.2c02051.
(25) Zhao, X.; Holta, D. E.; Tan, Z.; Oh, J.-H.; Echols, I. J.; Anas, M.; Cao, H.; Lutkenhaus, J. L.; Radovic, M.; Green, M. J. Annealed Ti3c2t Z Mxene Films for Oxidation-Resistant Functional Coatings. *ACS Appl. Nano Mater.* **2020**, *3* (11), 10578−10585.
(26) Natu, V.; Pai, R.; Sokol, M.; Carey, M.; Kalra, V.; Barsoum, M. W. 2d Ti3c2tz Mxene Synthesized by Water-Free Etching of Ti3alc2 in Polar Organic Solvents. *Chem.* **2020**, *6* (3), 616−630.
(27) Kotasthane, V.; Tan, Z.; Yun, J.; Pentzer, E. B.; Lutkenhaus, J. L.; Green, M. J.; Radovic, M. Selective Etching of Ti3alc2Max Phases Using Quaternary Ammonium Fluorides Directly Yields Ti3c2t Z. Mxene Nanosheets: Implications for Energy Storage. *ACS Appl. Nano Mater.* **2023**, *6*, 1093−1105, DOI: 10.1021/acsanm.2c04607.
(28) Lakhe, P.; Prehn, E. M.; Habib, T.; Lutkenhaus, J. L.; Radovic, M.; Mannan, M. S.; Green, M. J. Process Safety Analysis for Ti3c2t X Mxene Synthesis and Processing. *Ind. Eng. Chem. Res.* **2019**, *58* (4), 1570−1579.
(29) Urbankowski, P.; Anasori, B.; Makaryan, T.; Er, D.; Kota, S.; Walsh, P. L.; Zhao, M.; Shenoy, V. B.; Barsoum, M. W.; Gogotsi, Y. Synthesis of Two-Dimensional Titanium Nitride Ti 4 N 3 (Mxene). *Nanoscale* **2016**, *8* (22), 11385−11391.
(30) Kamysbayev, V.; Filatov, A. S.; Hu, H.; Rui, X.; Lagunas, F.; Wang, D.; Klie, R. F.; Talapin, D. V. Covalent Surface Modifications and Superconductivity of Two-Dimensional Metal Carbide Mxenes. *Science* **2020**, *369* (6506), 979−983.
(31) Li, M.; Lu, J.; Luo, K.; Li, Y.; Chang, K.; Chen, K.; Zhou, J.; Rosen, J.; Hultman, L.; Eklund, P.; et al. Element Replacement Approach by Reaction with Lewis Acidic Molten Salts to Synthesize Nanolaminated Max Phases and Mxenes. *J. Am. Chem. Soc.* **2019**, *141* (11), 4730−4737.
(32) Arole, K.; Blivin, J. W.; Bruce, A. M.; Athavale, S.; Echols, I. J.; Cao, H.; Tan, Z.; Radovic, M.; Lutkenhaus, J. L.; Green, M. J. Exfoliation, Delamination, and Oxidation Stability of Molten Salt Etched Nb 2 Ct Z Mxene Nanosheets. *Chem. Commun.* **2022**, *58* (73), 10202−10205.
(33) Arole, K.; Blivin, J. W.; Saha, S.; Holta, D. E.; Zhao, X.; Sarmah, A.; Cao, H.; Radovic, M.; Lutkenhaus, J. L.; Green, M. J. Water-Dispersible Ti3c2tz Mxene Nanosheets by Molten Salt Etching. *Iscience* **2021**, *24* (12), No. 103403.
(34) Li, Y.; Shao, H.; Lin, Z.; Lu, J.; Liu, L.; Duployer, B.; Persson, P. O.; Eklund, P.; Hultman, L.; Li, M.; et al. A General Lewis Acidic Etching Route for Preparing Mxenes with Enhanced Electrochemical Performance in Non-Aqueous Electrolyte. *Nat. Mater.* **2020**, *19*, 894−899.
(35) Yang, Y.-Y.; Zhou, W.-T.; Song, W.-L.; Zhu, Q.-Q.; Xiong, H.-J.; Zhang, Y.; Cheng, S.; Luo, P.-F.; Lu, Y.-W. Terminal Groups-Dependent near-Field Enhancement Effect of Ti3c2tx Nanosheets. *Nanoscale Res. Lett.* **2021**, *16* (1), No. 60.
(36) Maleski, K.; Mochalin, V. N.; Gogotsi, Y. Dispersions of Two-Dimensional Titanium Carbide Mxene in Organic Solvents. *Chem. Mater.* **2017**, *29* (4), 1632−1640.
(37) Schultz, T.; Frey, N. C.; Hantanasirisakul, K.; Park, S.; May, S. J.; Shenoy, V. B.; Gogotsi, Y.; Koch, N. Surface Termination Dependent Work Function and Electronic Properties of Ti3c2t X Mxene. *Chem. Mater.* **2019**, *31* (17), 6590−6597.
(38) Hart, J. L.; Hantanasirisakul, K.; Lang, A. C.; Anasori, B.; Pinto, D.; Pivak, Y.; van Omme, J. T.; May, S. J.; Gogotsi, Y.; Taheri, M. L.

Control of Mxenes' Electronic Properties through Termination and Intercalation. *Nat. Commun.* **2019**, *10* (1), No. 522.
(39) Kim, H.; Alshareef, H. N. Mxetronics: Mxene-Enabled Electronic and Photonic Devices. *ACS Mater. Lett.* **2020**, *2* (1), 55−70.
(40) Halim, J.; Cook, K. M.; Naguib, M.; Eklund, P.; Gogotsi, Y.; Rosen, J.; Barsoum, M. W. X-Ray Photoelectron Spectroscopy of Select Multi-Layered Transition Metal Carbides (Mxenes). *Appl. Surf. Sci.* **2016**, *362*, 406−417.
(41) Natu, V.; Benchakar, M.; Canaff, C.; Habrioux, A.; Celerier, S.; Barsoum, M. W. A Critical Analysis of the X-Ray Photoelectron Spectra of Ti3c2tz Mxenes. *Matter* **2021**, *4*, 1224−1251, DOI: 10.1016/j.matt.2021.01.015.
(42) Verger, L.; Xu, C.; Natu, V.; Cheng, H.-M.; Ren, W.; Barsoum, M. W. Overview of the Synthesis of Mxenes and Other Ultrathin 2d Transition Metal Carbides and Nitrides. *Curr. Opin. Solid State Mater. Sci.* **2019**, *23* (3), 149−163.
(43) Kotasthane, V.; Holta, D. E.; Zhao, X.; Lutkenhaus, J. L.; Green, M. J.; Radovic, M. Core−Shell Mechanism of Etching V2alc Max Phase to V2ct Z Mxenes. *J. Mater. Res.* **2023**, *38* (6), 1527−1542.
(44) Li, Z.; Wang, L.; Sun, D.; Zhang, Y.; Liu, B.; Hu, Q.; Zhou, A. Synthesis and Thermal Stability of Two-Dimensional Carbide Mxene Ti3c2. *Mater. Sci. Eng., B* **2015**, *191*, 33−40.
(45) Tang, M.; Li, J.; Wang, Y.; Han, W.; Xu, S.; Lu, M.; Zhang, W.; Li, H. Surface Terminations of Mxene: Synthesis, Characterization, and Properties. *Symmetry* **2022**, *14* (11), No. 2232.
(46) Abdolhosseinzadeh, S.; Jiang, X.; Zhang, H.; Qiu, J.; Zhang, C. J. Perspectives on Solution Processing of Two-Dimensional Mxenes. *Mater. Today* **2021**, *48*, 214−240, DOI: 10.1016/j.mattod.2021.02.010.
(47) Kailasa, S. K.; Joshi, D. J.; Koduru, J. R.; Malek, N. I. Review on Mxenes-Based Nanomaterials for Sustainable Opportunities in Energy Storage, Sensing and Electrocatalytic Reactions. *J. Mol. Liq.* **2021**, *342*, No. 117524.
(48) Zhao, X.; Vashisth, A.; Prehn, E.; Sun, W.; Shah, S. A.; Habib, T.; Chen, Y.; Tan, Z.; Lutkenhaus, J. L.; Radovic, M. Antioxidants Unlock Shelf-Stable Ti3c2tx (Mxene) Nanosheet Dispersions. *Matter* **2019**, *1*, 513−526, DOI: 10.1016/j.matt.2019.05.020.
(49) Chen, J.; Yuan, X.; Lyu, F.; Zhong, Q.; Hu, H.; Pan, Q.; Zhang, Q. Integrating Mxene Nanosheets with Cobalt-Tipped Carbon Nanotubes for an Efficient Oxygen Reduction Reaction. *J. Mater. Chem. A* **2019**, *7* (3), 1281−1286.
(50) Ji, J.; Zhao, L.; Shen, Y.; Liu, S.; Zhang, Y. Covalent Stabilization and Functionalization of Mxene Via Silylation Reactions with Improved Surface Properties. *FlatChem.* **2019**, *17*, No. 100128.
(51) Riazi, H.; Anayee, M.; Hantanasirisakul, K.; Shamsabadi, A. A.; Anasori, B.; Gogotsi, Y.; Soroush, M. Surface Modification of a Mxene by an Aminosilane Coupling Agent. *Adv. Mater. Interfaces* **2020**, *7* (6), No. 1902008.
(52) Sangu, S. S.; Illias, N. M.; Ong, C. C.; Gopinath, S. C. B.; Saheed, M. S. M. Mxene-Based Aptasensor: Characterization and High-Performance Voltammetry Detection of Deoxynivalenol. *BioNanoScience* **2021**, *11* (2), 314−323.
(53) Rosenkranz, A.; Grützmacher, P. G.; Espinoza, R.; Fuenzalida, V. M.; Blanco, E.; Escalona, N.; Gracia, F. J.; Villarroel, R.; Guo, L.; Kang, R.; et al. Multi-Layer Ti3c2tx-Nanoparticles (Mxenes) as Solid Lubricants−Role of Surface Terminations and Intercalated Water. *Appl. Surf. Sci.* **2019**, *494*, 13−21.
(54) Miao, X.; Li, Z.; Liu, S.; Wang, J.; Yang, S. Mxenes in Tribology: Current Status and Perspectives. *Adv. Powder Mater.* **2023**, *2*, No. 100092.
(55) Marian, M.; Song, G. C.; Wang, B.; Fuenzalida, V. M.; Krauß, S.; Merle, B.; Tremmel, S.; Wartzack, S.; Yu, J.; Rosenkranz, A. Effective Usage of 2d Mxene Nanosheets as Solid Lubricant−Influence of Contact Pressure and Relative Humidity. *Appl. Surf. Sci.* **2020**, *531*, No. 147311.
(56) Grützmacher, P. G.; Suarez, S.; Tolosa, A.; Gachot, C.; Song, G.; Wang, B.; Presser, V.; Mücklich, F.; Anasori, B.; Rosenkranz, A. Superior Wear-Resistance of $Ti_3c_2t_X$ Multilayer Coatings. *ACS Nano* **2021**, *15* (5), 8216−8224.
(57) Boidi, G.; de Queiróz, J. C. F.; Profito, F. J.; Rosenkranz, A. $Ti_3c_2t_X$ Mxene Nanosheets as Lubricant Additives to Lower Friction under High Loads, Sliding Ratios, and Elevated Temperatures. *ACS Appl. Nano Mater.* **2022**, *6*, 729−737, DOI: 10.1021/acsanm.2c05033.
(58) Wyatt, B. C.; Rosenkranz, A.; Anasori, B. 2d Mxenes: Tunable Mechanical and Tribological Properties. *Adv. Mater.* **2021**, *33* (17), No. 2007973.
(59) Samanta, S.; Singh, S.; Sahoo, R. R. Covalently Grafting of Self-Assembled Functionalized Graphene Oxide Multilayer Films on Si Substrate for Solid Film Lubrication. *Thin Solid Films* **2019**, *683*, 16−26.
(60) Dai, W.; Kheireddin, B.; Gao, H.; Liang, H. Roles of Nanoparticles in Oil Lubrication. *Tribiol. Int.* **2016**, *102*, 88−98.
(61) Dašić, P.; Franek, F.; Assenova, E.; Radovanović, M. *International Standardization and Organizations in the Field of Tribology*; Emerald Group Publishing Ltd., 2003; *55*, pp 287−291.
(62) Rosenkranz, A.; Righi, M. C.; Sumant, A. V.; Anasori, B.; Mochalin, V. N. Perspectives of 2d Mxene Tribology. *Adv. Mater.* **2023**, *35* (5), No. 2207757.
(63) Feng, Q.; Deng, F.; Li, K.; Dou, M.; Zou, S.; Huang, F. Enhancing the Tribological Performance of Ti3c2Mxene Modified with Tetradecylphosphonic Acid. *Colloids Surf., A* **2021**, *625*, No. 126903.

https://doi.org/10.1021/acsami.3c18232
ACS Appl. Mater. Interfaces 2024, 16, 6290−6300